Reduction of Eddy-Current-Induced Distortion in Diffusion MRI Using a Twice-Refocused Spin Echo

T.G. Reese,[1*] O. Heid,[2] R.M. Weisskoff,[3] and V.J. Wedeen[1]

Image distortion due to field gradient eddy currents can create image artifacts in diffusion-weighted MR images. These images, acquired by measuring the attenuation of NMR signal due to directionally dependent diffusion, have recently been shown to be useful in the diagnosis and assessment of acute stroke and in mapping of tissue structure. This work presents an improvement on the spin-echo (SE) diffusion sequence that displays less distortion and consequently improves image quality. Adding a second refocusing pulse provides better image quality with less distortion at no cost in scanning efficiency or effectiveness, and allows more flexible diffusion gradient timing. By adjusting the timing of the diffusion gradients, eddy currents with a single exponential decay constant can be nulled, and eddy currents with similar decay constants can be greatly reduced. This new sequence is demonstrated in phantom measurements and in diffusion anisotropy images of normal human brain. **Magn Reson Med 49:177–182, 2003.** © 2003 Wiley-Liss, Inc.

Key words: diffusion MRI; eddy currents; image distortion; pulse sequence; artifact

Multidirectional diffusion sequences (1–3) have recently been shown to be useful in the diagnosis and assessment of acute stroke and in mapping of tissue structure (4–10). These methods apply gradient pulses at higher intensity and with longer duration than in any other well known MRI sequence, resulting in comparatively large and persistent eddy currents. Use of the spin-echo (SE) diffusion sequence with an echo planar (EP) readout combines atypically large eddy currents with an eddy current-sensitive EP readout, causing spatial distortion dependent on the direction of the applied diffusion gradient. Misregistration artifacts result when directional diffusion is calculated from multiple images with differing gradient directions.

Each on and off field gradient transition produces eddy currents to some degree. If the eddy current (and its associated magnetic field) decays to an inconsequential value between the time of the applied field gradient transition and the image readout, a spatially dependent change in image phase will result with no discernible distortion. Since diffusion encoding relies on the attenuation of the image magnitude, a change in image phase does not change the diffusion measurement as long as the phase

gradient per pixel is small (11). However, when the eddy current decays slowly, so that a residual field remains during the image readout, the field behaves like an additional spatial encoding gradient field and causes distortion of the image.

While the usual SE diffusion sequence, introduced by Stejkal and Tanner (12), uses a single refocusing RF pulse, many SE diffusion sequence variants can be created using multiple refocusing pulses. SEs result from any combination of refocusing pulses that returns the spins' phase evolution to the origin in classical phase space (13). Using more than one refocusing pulse permits variable intervals between the pulses, requiring only that the spins' alternating defocusing and refocusing times sum equally at the time of the intended SE. This flexibility in timing adds utility when used for diffusion imaging.

Since the on and off field gradient transitions produce equal and opposite eddy currents, the shorter the time between on and off transitions, the less decay of the residual fields during the gradient pulse and the more complete the fields' cancellation. Toward this end, a reduction of distortion can be affected by adding additional RF refocusing pulses to the SE diffusion sequence, splitting the field gradient pulses into shorter pulses of alternating polarity (14). By adding the additional refinement of unequal and asymmetric lengths to these shorter pulses, specific exponentially decaying residual fields can be entirely canceled (15). The twice-refocused SE (TRSE) sequence described in the present work compromises neither efficiency or effectiveness compared to the singly-refocused Stejkal-Tanner SE sequence, while greatly reducing eddy distortion.

METHODS

An SE diffusion sequence with two refocusing pulses forms the TRSE sequence as shown in Fig. 1. Two bipolar field gradients of length $\delta_1 + \delta_2$ and $\delta_3 + \delta_4$, are used, with the RF refocusing pulses dividing each bipolar pair. Consider an idealized sequence, in which the RF pulse durations and gradient ramping times are infinitely short, then

$$\delta_1 + \delta_2 = \delta_3 + \delta_4$$

$$\delta_2 + \delta_3 = TE/2$$

$$\delta_1 + \delta_4 = TE/2 - t_{pr} \qquad [1]$$

where t_{pr} is the sum of the preparation time following the excitation pulse and the readout time preceding the SE. Three equations with four unknowns leaves one free parameter, here chosen to be δ_4. Because of the timing flexibility afforded by the second refocusing pulse, all the

---

[1]Department of Radiology, Massachusetts General Hospital, Boston, Massachusetts.
[2]Medical Engineering Division, Siemens AG, Erlangen, Germany.
[3]Epix Medical Inc., Cambridge, Massachusetts.
*Correspondence to: Timothy G. Reese, Ph.D., MGH NMR Center, Building 149, 13th Street (2301), Charlestown Navy Yard, Charlestown, MA 02129. E-mail: reese@nmr.MGH.harvard.edu
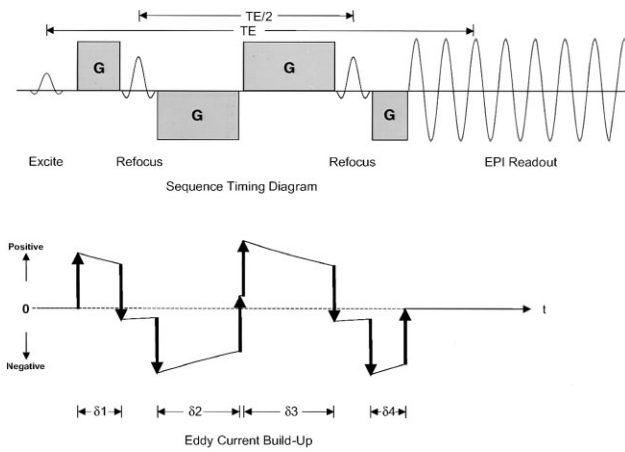
FIG. 1. The TRSE sequence is shown as a timing diagram. The RF pulses (excite and refocus), diffusion gradients **G** of lengths δ_1, δ_2, δ_3, and δ_4, and the EP readout are shown; other sequence elements are omitted for clarity. The sequence allows any diffusion gradient lengths such that the time between the two refocusing pulses is TE/2, and the dephasing and rephasing due to the diffusion gradients are equal. The graph below the timing diagram shows the buildup and decay of eddy currents due to the gradient switching. The on and off diffusion gradient transitions that generate the eddy currents are shown with bold black arrows. With knowledge of the principle eddy current decay time constant λ, diffusion gradient lengths can be calculated so that eddy current buildup is nulled prior to readout. The proportions of gradient lengths in this figure match the actual durations of gradients at the eddy current null shown in Fig. 2.

available time between the imaging sequence elements can be filled with diffusion-encoding field gradient pulses.

Diffusion scans were acquired with both GE Signa (General Electric Medical Systems, Milwaukee WI) and Siemens Sonata (Siemens Medical Systems, Erlangen, Germany) 1.5T clinical MR instruments using single-excitation EPI. The GE Signa was equipped with an Instascan EPI retrofit (Advanced NMR, Wilmington MA). The image matrix size was 128×128, with an FOV of 256×256 mm, and a slice thickness of 5 mm. Maximum gradient strength for the Signa was 10 mT/m with a slewing time of 60 μs/mT/m for conventional gradients, and 32 mT/m with a maximum of 4 μs/mT/m for the EPI readout gradient. The maximum gradient amplitude for the Sonata system is 40 mT/m with a rise time of 5 μs/mT/m. Acquisition time was 512 μs per line of data, covering 75% of the phase-encoding axis. Magnitude reconstruction was completed at the console, with additional processing completed offline.

Phantom data using the Sonata were acquired of 24 slices with a 256-mm FOV over a 20-cm-diameter water sphere, 5 mm thickness, and a 2.5-mm gap with $B = 1000$ s/mm^2, TE = 88 ms, and TR = 4800 ms. Data were collected in the three cardinal axes (axial, sagittal, and coronal) plus unencoded (T_2 weighted) with the TRSE sequence while varying the diffusion field gradient timing by 1-ms steps across the available range (1–15 ms). A Stejkal-Tanner sequence with the same diffusion weighting and TE was similarly tested.

Normal volunteers were scanned with informed consent on the Signa and Sonata under an IRB-approved protocol

using the Stejkal-Tanner SE and the TRSE sequence with nominal diffusion field gradient timing. Scan timing was as in the phantom scans but utilizing multiaxis tensor encoding (six field gradient axes plus T_2 weighted). Tensor analysis was carried out using software written by the authors and their colleagues for this purpose.

RESULTS

Misregistration between the phantom images collected with n different diffusion encoding axes, but with the same sequence type and timing, was evaluated by calculating the variance σ^2 for each pixel magnitude m at location $\mathbf{x}$ and for sequence timing δ_4,

$$\sigma^2(\mathbf{x},\delta_4) = \frac{1}{n-1} \sum_n (\bar{m}(\mathbf{x},\delta_4) - m_n(\mathbf{x},\delta_4))^2. \qquad [2]$$

Summed pixel variance for each slice, timing, and sequence type was displayed on a 3D plot, showing the timing and sequence type that exhibits the best registration across all slices (Fig. 2).

From the timing of the sequence parameters giving the best registration using the TRSE sequences, the principle time constant of the residual eddy currents can be determined. Assuming a dominant monoexponential decay, we can model the residual field due to the eddy currents as the superposition of fields resulting from the on and off transitions of the diffusion-encoding gradient fields. The resultant field is then a linearly-variant in space, exponentially decaying change in the static field B_0.

$$B(\mathbf{x},t) = B_0 + \Delta B(\mathbf{x},t) = B_0 + |\Delta B| \cdot \mathbf{x} \sum_n s(n)\exp[(\tau_n - t)/\lambda]$$

$$[3]$$

Let ΔB be equal and opposite for the on and off transitions of the field gradient waveform with $s(n)$ the sign of the transition, τ_n the time of the nth transition, t sometime during the readout, and λ the time constant of decay. The principle time constant λ of the residual field decay can be determined numerically from the sequence timing that gives the minimum variance in pixel registration, i.e., λ, such that $\sum_\mathbf{x}\sigma^2(\mathbf{x},\delta_4) \to 0$. There exists a unique solution to $\sum_n s(n)\exp[(\tau_n - t)/\lambda] = 0$ for realistic values of τ_n, λ, and t. These findings are shown graphically in Fig. 2, and the calculated time constants λ are shown in Table 1.

Diffusion tensor MRI of normal human subjects was collected for subjective comparison of the Stejkal-Tanner and TRSE sequences. Tensor images of diffusion attenuation were calculated; contrast in these images demonstrates directional diffusion anisotropy (Fig. 3). Misregistration in the diffusion images can generate anomalous contrast due to the comparison of dissimilar materials in the same pixel. The image misregistration is most apparent at the tissue–air interface surrounding the head. Here the comparison of pixels in air with eddy-current-shifted tissue pixels between differing gradient directions produces
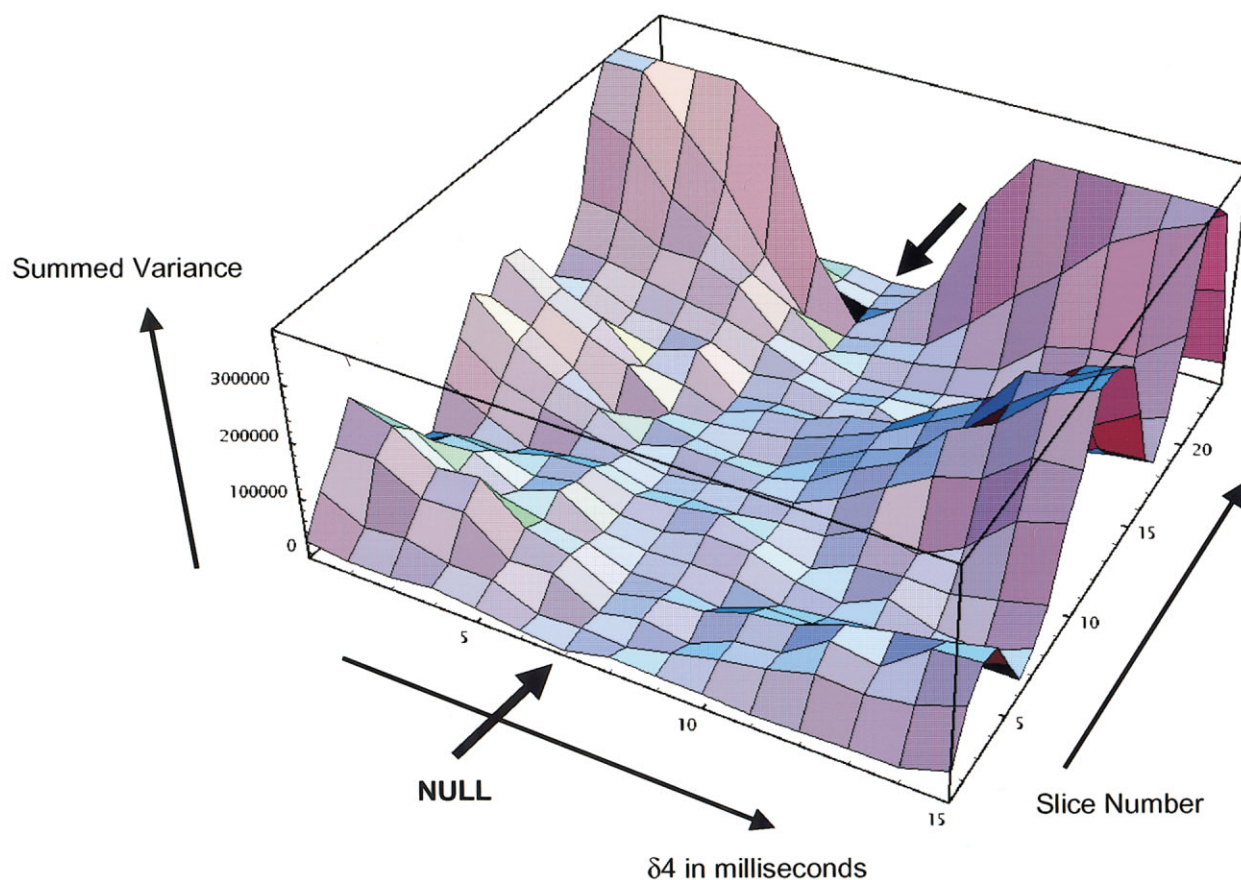
FIG. 2. Eddy current-induced misregistration can be measured as the variance in pixel-by-pixel image intensity of a stationary homogeneous object encoded with different diffusion directions. Increased variance indicates misregistration. A spherical water phantom 20 cm in diameter was imaged with 24 5-mm slices with diffusion encoding in each of the three cardinal axes (x, y, and z). The *B*-value was 1000 s/mm^2 and the TE was 88 ms. The summed variance between x, y, and z for all pixels in each transverse plane slice and each possible sequence timing is shown in this figure. The eddy current minimum (null) appears at 7 ms. The Stejkal-Tanner SE sequence gave about three times more variance than the worst-case TRSE timing.

large amounts of contrast unrelated to tissue diffusion anisotropy. This spurious contrast can also be seen in the gray matter; white/gray diffusion contrast clearly improves with better image registration evident with the TRSE sequence. Blurring and displacement of fine white matter structure is also reduced with TRSE.

DISCUSSION

Due to its long readout times, EPI is particularly susceptible to eddy-current-induced image distortion. Residual fields that are constant across the FOV produce an image translation along the phase-encode axis just as an off-

Table 1

Variance in Three Slice Axes Due to Misregistration of the Cardinal Diffusion Axes, Summed Over All 24 Slices for Each Adjustment of Timing Given in the Methods

	Stejkal-Tanner SE variance (in millions)	Minimum TRSE variance	Maximum TRSE variance	Idealized λ	Numerically calculated λ
Transverse	17 (1:1)	0.23 (73:1)	5.2 (3.2:1)	37 ms	30 ms
Sagittal	11 (1:1)	0.75 (14:1)	4.5 (2.4:1)	divergent	divergent
Coronal	13 (1:1)	0.34 (37:1)	2.7 (4.8:1)	51 ms	40 ms

The variance is shown in millions of units, and the ratio of improvement over the Stejkal-Tanner sequence is shown following the TRSE variance values in parentheses. Time constants λ were calculated from the zero intercept of a linear fit of the variances with δ_4 equal to from 1 to 6 ms. λ was calculated by Newton's method from the idealized sequence timing (zero rf pulse length and zero gradient ramp time) due to Heid (15), while the numeric value was calculated from the actual sequence timing. All axes had a δ_4 setting with a clear minimum in variance (7 ms for transverse and coronal, 9 ms for sagittal), although the sagittal axis does not fit the monoexponential model well enough to provide a meaningful value of λ.
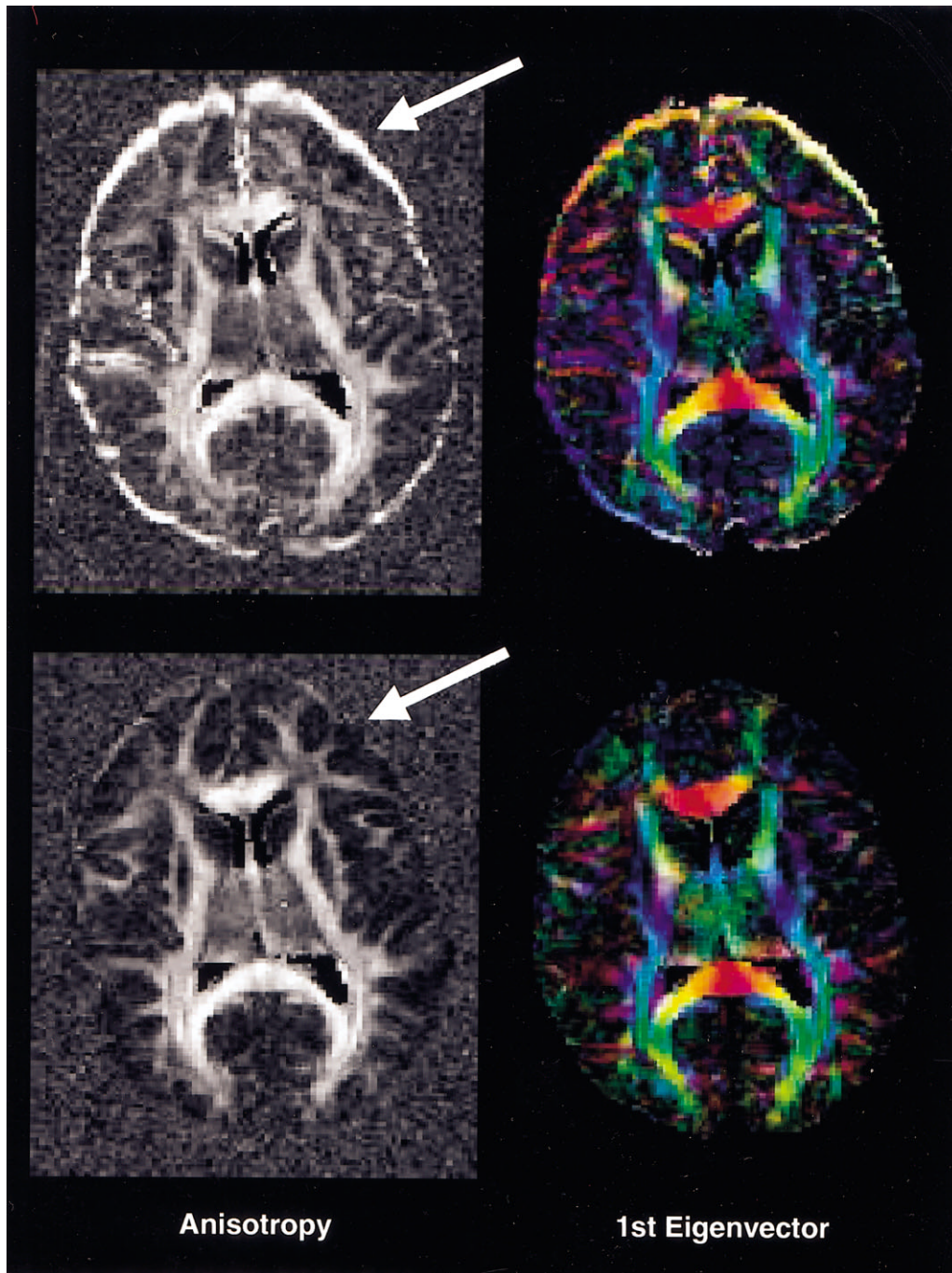
FIG. 3. Comparison of Stejkal-Tanner and TRSE sequences in diffusion tensor MRI of the human brain. Typical GE/Instascan images from the same level in the midbrain are shown. The usual Stejkal-Tanner SE diffusion sequence was used for the upper pair of images, and the TRSE sequence was used for the lower pair. The T_2-weighted images of this slice from each sequence type are indistinguishable. Diffusion anisotropy (29) is shown as the grayscale images on the left. The first eigenvector of the diffusion tensor are in color at the right. The eigenvectors, calculated and displayed as in Wiegell et al. (10), shows the direction of the eigenvector as red, green, and blue, with the degree of anisotropy given by the color intensity. Pixels in the color eigenvector images without significant diffusion anisotropy have been masked. The arrows point to regions of anomalous diffusion contrast resulting from misregistration of dissimilar materials. Note the prominent edge artifact visible in the Stejkal-Tanner SE images, which is almost entirely absent in the TRSE images. Improved image registration with TRSE also clarifies anatomy by removing artifactual contrast.

resonance condition would. Residual fields can also mirror the first-order spatial dependence of the applied gradient fields. The archetypical skew distortion (a stretching or shrinking along the image diagonal) of less than 3.125 mm

(nominally 1 pixel) in the EP readout axis requires a very small additional field; for an image with $N = 128$ lines,

$$\gamma G_{\text{eddy}} NT = \frac{\gamma}{128} \frac{2}{\pi} G_{\text{epi}} T \text{ and } G_{\text{eddy}} < \frac{1}{128} \frac{2}{\pi N} G_{\text{epi}} = 1.5$$

$\times\ 10^{-3}$mT/m, or less than 0.005% of the applied gradient, where T is the readout time and the imaging gradient G_{epi} is 40 mT/m.

To minimize eddy currents resulting from MRI pulse sequences, several methods are widely employed. The gradient coil can be designed to minimize its electromagnetic coupling with any conductive parts in the magnet cryostat and surround (16,17). Another approach, called "active eddy compensation" or "gradient preemphasis" (18,19), compensates for eddy currents by changing the shape of the field gradient amplitude envelope to anticipate the combined intended and residual fields. Both methods are now common in high-performance MRI systems. One can also modify the image data to undo the effects of the additional gradient fields due to eddy currents, as in Refs. 20–25. Although most investigators can access this correction, the method entails added noise and processing time, and requires manual recalibration for changes in sequence timing.

The method described here minimizes the effects of eddy currents by changing the design of the pulse sequence. Several authors have designed sequences that strive to minimize eddy currents. Boesch et al. (19) proposed adding gradient prepulses to partly compensate for residual fields due to the subsequent encoding gradients. Replacement of long constant gradients with bipolar gradients has been used in diffusion spectroscopy (26,27), and in diffusion imaging (28) to reduce eddy current buildup. To our knowledge, the sequence described here and in Ref. 15 is the first to null residual fields of a specific time constant, with no loss of scanning efficiency. Although one of the authors has presented a closed-form solution for sequence timing based on knowing the dominant residual field decay constant λ and the idealized sequence timing (zero length RF pulses, zero gradient ramp time; see Ref. 15), one would not typically know λ prior to implementation of the TRSE sequence. In the present work, the sequence itself was used to determine the best timing to minimize distortion, and λ was calculated numerically from the sequence timing. Differences between λ calculated using an idealized sequence (zero RF pulse length, zero gradient ramp time) and the actual sequence timing were about 15% (Table 1). Using λ, the nominal TRSE sequence timing for any B-value can be calculated.

More efficient sequence timing with TRSE offsets any time penalty due to the additional refocusing pulse. A simple comparison using idealized sequence timing (zero RF pulse length, zero gradient ramp time) shows that the TRSE sequence will always be more efficient (i.e., shorter TE for the same B-value) than the Stejkal-Tanner SE for realistic readout times. Define t_r as the readout time before the echo, and t_p as the gradient preparation time after the excitation pulse. Then

$$\frac{B_{TR}}{B_{ST}} = \left[\frac{TE - t_r - t_p}{TE - 2t_r} \right]^3 > 0 \quad \text{iff} \quad t_r > t_p \qquad [4]$$

where $\boldsymbol{B}_{ST}$ is the B-value of the Stejkal-Tanner SE sequence and $\boldsymbol{B}_{TR}$ is the B-value of the TRSE sequence for a given TE. For example, a Stejkal-Tanner SE sequence with a B of 1000, t_r of 16 ms, gradient strength of 40 mT/m, and a refocusing pulse length of 4 ms will have a TE of about 76 ms. A similar TRSE sequence with a t_p of 4 ms and a δ_4 of 7 ms will have a TE of 59 ms—a 22% decrease in TE.

As can be seen in the phantom data (Fig. 2) for our Sonata system, the dominant time constant is sufficiently distinct to allow cancellation of the majority of eddy distortion by nulling a single time constant. Fortunately, the cancellation function has a broad minimum around the putative null; thus the majority of benefit can be achieved without precise characterization of eddy current spatial and temporal distribution. As shown in the phantom data from our Sonata, different image orientations have slightly different putative nulls. This likely results from a superposition of eddy currents with slightly different decay constants, each with a different spatial distribution, and each more or less dominant depending on the orientation of the image axes. In the tested cases, the worst-case timing for TRSE produced about one-third of the misregistration variance of a Stejkal-Tanner SE diffusion sequence with equal B and similar timing.

Additional new sequence designs to cancel eddy currents of more than one decay constant can be formed by adding more refocusing pulses. Each additional pulse provides an additional degree of freedom, and could simultaneously cancel eddy currents with different decay constants. Although feasible, practicality issues such as added complexity, necessarily longer TEs, increased RF power deposition, the need for characterization of spatial dependence, and the presence of parasitic echoes make the implementation and use of such sequences uncertain.

CONCLUSIONS

We have presented a method to improve multidirectional diffusion images by reducing spatial distortion caused by eddy currents. Addition of a second refocusing pulse to the SE-EPI sequence changes the timing and number of diffusion-encoding gradient pulses. Distortion is reduced by adjusting the new sequence's timing to null eddy currents with a single time constant. We have demonstrated improved image quality using the new sequence without any loss of scanning efficiency or effectiveness, and without any calibration and/or correction of images.

REFERENCES

1. van Gelderen P, de Vleeschouwer MH, DesPres D, Pekar J, van Zijl PC, Moonen CT. Water diffusion and acute stroke. Magn Reson Med 1994; 31:154–163.
2. Basser PJ, Mattiello J, LeBihan D. MR diffusion tensor spectroscopy and imaging. Biophys J 1994;66:259–267.
3. Wedeen VJ, Reese TG, Tuch DS, Weigell MR, Dou J-G, Weisskoff RM, Chesler D. Mapping fiber orientation spectra in cerebral white matter with Fourier-transform diffusion MRI. In: Proceedings of the 8th Annual Meeting of ISMRM, Denver, 2000. p 82.
4. Garrido L, Wedeen VJ, Kwong KK, Spencer UM, Kantor HL. Anisotropy of water diffusion in the myocardium of the rat. Circ Res 1994;74:789–793.
5. Pierpaoli C, Jezzard P, Basser PJ, Barnett A, Di Chiro G. Diffusion tensor MR imaging of the human brain. Radiology 1996;201:637–648.
6. Reese TG, Weisskoff RM, Smith RN, Rosen BR, Dinsmore RE, Wedeen VJ. Imaging myocardial fiber architecture in vivo with magnetic resonance. Magn Reson Med 1995;34:786–791.

7. Sorensen AG, Wu O, Copen WA, Davis TL, Gonzalez RG, Koroshetz WJ, Reese TG, Rosen BR, Wedeen VJ, Weisskoff RM. Human acute cerebral ischemia: detection of changes in water diffusion anisotropy by using MR imaging. Radiology 1999;212:785–792.

8. Tuch DS, Wedeen VJ, Dale AM, George JS, Belliveau JW. Conductivity mapping of biological tissue using diffusion MRI. Ann NY Acad Sci 1999;888:314–316.

9. Wedeen VJ, Reese TG, Napadow VJ, Gilbert RJ. Demonstration of primary and secondary muscle fiber architecture of the bovine tongue by diffusion tensor magnetic resonance imaging. Biophys J 2001;80:1024–1028.

10. Weigell MR, Larsson HB, Wedeen VJ, Reese TG, Napadow VJ, Gilbert RJ. Fiber crossing in human brain depicted with diffusion tensor MR imaging. Radiology 2000;217:897–903.

11. Wedeen VJ, Weisskoff RM, Poncelet BP. MRI signal void due to in-plane motion is all-or-none. Magn Reson Med 1994;32:116–120.

12. Stejkal EO, Tanner JE. Spin diffusion measurements: spin echoes in the presence of a time-dependent field gradient. J Chem Phys 1965;41:288–292.

13. Waugh JS, Rhim W-K, Pines A. Spin echoes and Loschmidt's paradox. J Magn Reson 1972;6:317–324.

14. Reese TG, Weisskoff RM, Wedeen VJ. Diffusion NMR facilitated by a refocused eddy-current EPI pulse sequence. In: Proceedings of the 6th Annual Meeting of ISMRM, Sydney, Australia, 1998. p 663.

15. Heid O. Eddy current-nulled diffusion weighting. In: Proceedings of the 8th Annual Meeting of ISMRM, Denver, 2000. p 799.

16. Bowtell R, Mansfield P. Gradient coil design using active magnetic screening. Magn Reson Med 1991;17:15–19; discussion 19–21.

17. Roemer PB, Edelstein WA, Hickey JM. Active magnet shielding of gradient coils in NMR imaging. In: Proceedings of the 5th Annual Meeting of SMRM, Montreal, Canada, 1986. p 1067.

18. Ahn CB, Cho ZH. Analysis of eddy currents induced artifacts and temporal compensation in nuclear magnetic resonance imaging. IEEE Trans Med Imaging 1991;10:47–52.

19. Boesch C, Gruetter R, Martin E. Temporal and spatial analysis of fields generated by eddy currents in superconducting magnets: optimization of corrections and quantitative characterization of magnet/gradient systems. Magn Reson Med 1991;20:268–284.

20. Bastin ME. Correction of eddy current-induced artefacts in diffusion tensor imaging using iterative cross-correlation. Magn Reson Imaging 1999;17:1011–1024.

21. Calamante F, Porter DA, Gadian DG, Connelly A. Correction for eddy current induced B_0 shifts in diffusion-weighted echo-planar imaging. Magn Reson Med 1999;41:95–102.

22. Chen NK, Wyrwicz AM, Bastin ME. Optimized distortion correction technique for echo planar imaging. Magn Reson Med 2001;45:525–528.

23. Haselgrove JC, Moore JR, Pierpaoli C, Jezzard P, Basser PJ, Barnett A, Di Chiro G. Correction for distortion of echo-planar images used to calculate the apparent diffusion coefficient. Magn Reson Med 1996;36:960–964.

24. Horsfield MA. Mapping eddy current induced fields for the correction of diffusion-weighted echo planar images. Magn Reson Imaging 1999;17:1335–1345.

25. Jezzard P, Barnett AS, Pierpaoli C. Characterization of and correction for eddy current artifacts in echo planar diffusion imaging. Magn Reson Med 1998;39:801–812.

26. Fordham EJ, Gibbs SJ, Hall LD. Partially restricted diffusion in a permeable sandstone: observations by stimulated echo PFG NMR. Magn Reson Imaging 1994;12:279–284.

27. Wu D, Chen A, Johnson CS. An improved diffusion-ordered spectroscopy experiment incorporating bipolar-gradient pulses. J Magn Reson A 1995;115:260–264.

28. Alexander AL, Tsuruda JS, Parker DL. Elimination of eddy current artifacts in diffusion weighted echo-planar images: the use of bipolar gradients. Magn Reson Med 1997;38:1016–1021.

29. Basser PJ, Pierpaoli C. Microstructural and physiological features of tissues elucidated by quantitative-diffusion-tensor MRI. J Magn Reson B 1996;111:209–219.